

Supplementary Materials for

A natural gain strategy of passive cycling water vapour escape toward efficient freshwater purification

Lintao Mi^{1,2,3}, Zhiwen Zhang^{1,2,3}, Xingli Zhang^{1,2,3}, Chuanlong Han^{1,2}, Wensheng Wang^{1,2}, Wenlong Song^{1,2,}, Zhuangzhi Sun^{1,2,*}*

¹ Province Key Laboratory of Forestry Intelligent Equipment Engineering, College of Mechanical and Electrical Engineering, Northeast Forestry University, Harbin 150000, People's Republic of China.

² Key Laboratory of Biobased Material Science & Technology, Ministry of Education, Northeast Forestry University, Harbin 150000, People's Republic of China.

³ These authors contributed equally to this work.

* Corresponding authors. Email: sunzhuangzhi@nefu.edu.cn; swl@nefu.edu.cn

Brief description of what this file includes:

Supplementary Figure 1. CNT distribution on the surface of CNT/non-woven fabric.

Supplementary Figure 2. Numerical simulation of TIE flow field and humidity field.

Supplementary Figure 3. Flow field visualization.

Supplementary Figure 4. Structural simplification design for convective visualization.

Supplementary Figure 5. The infrared images of evaporation in the TIE or the TIE without flow.

Supplementary Figure 6. The temperature changes in the photothermal area under low sun intensity.

Supplementary Figure 7. The advantages and performance comparison of CNT/non-woven fabrics.

Supplementary Figure 8. The salt distribution of the TIE after long-term evaporation under seawater conditions.

Supplementary Figure 9. The overall design of the solar chimney.

Supplementary Figure 10. The initial idea of water vapour condensation and collection.

Supplementary Figure 11. 3D printing framework of the TIE.

Supplementary Table 1. List of materials for the solar chimney.

Supplementary Note 1. Ideal gas law and Dalton's law.

Supplementary Note 2. Numerical simulation.

References.

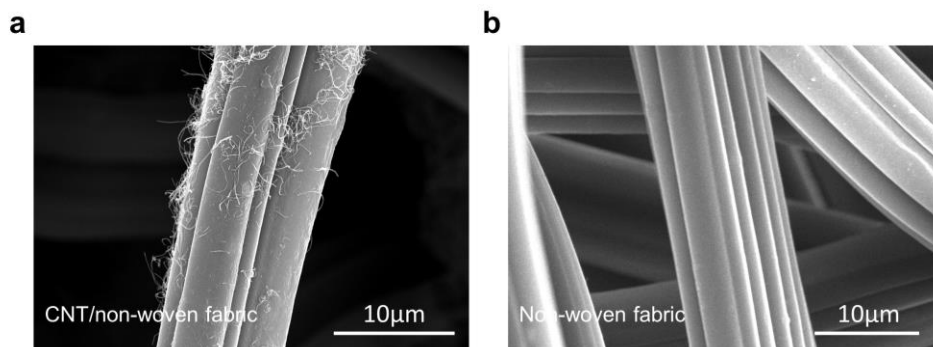


Figure S1. The SEM images of CNT/non-woven fabric and non-woven fabric. (a) the dispersion of CNT in the CNT/non-woven fabrics. (b) Enlarged image of non-woven fabrics.

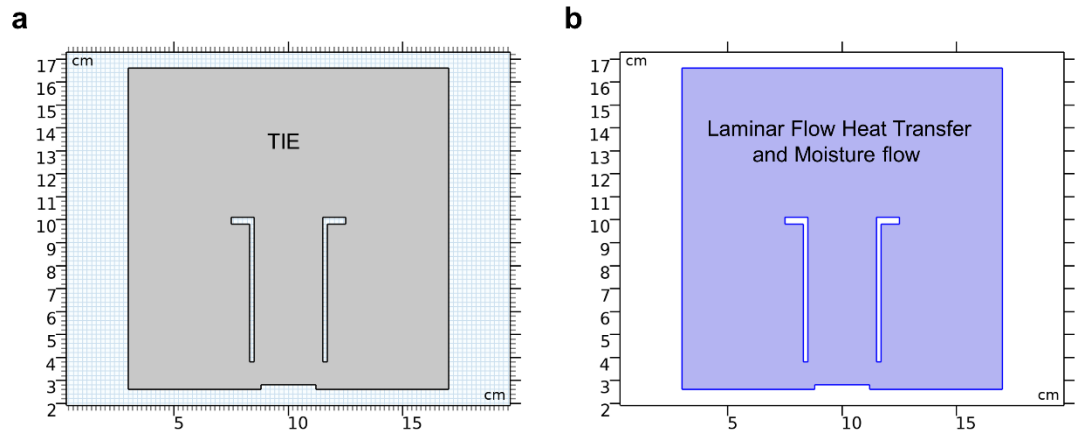


Figure S2. Numerical simulation of TIE flow field and humidity field. (a) TIE numerical simulation of geometric dimensions. (b) TIE numerical simulation of physical fields.

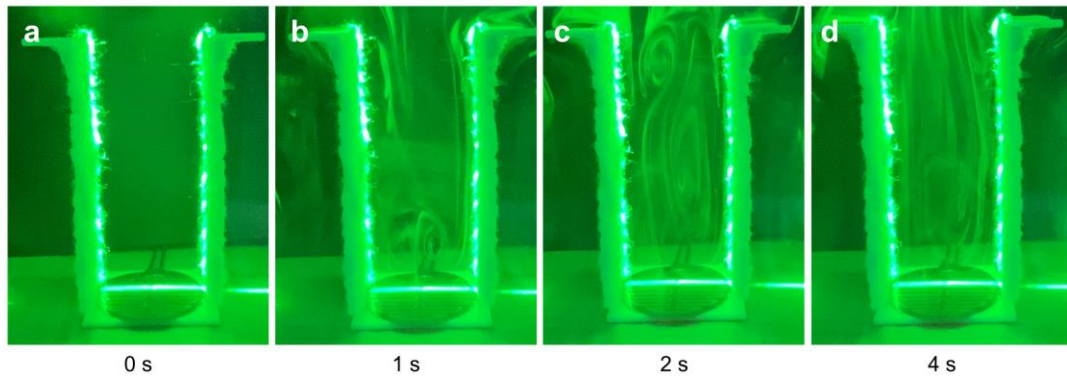


Figure S3. Flow field visualization. (a)- (d) Instantaneous change of natural convection inside the TIE. Smoke visualization technology can characterize the vapour flow field within the TIE, helping to reveal structural/operational defects and achieve optimized design. Compared to CFD simulation, visualization experiments capture the flow pattern of vapour more reliably and reveal the flow characteristics more intuitively. Smoke particles are considered ideal tracers because they have better reflectivity and little or only slight impact on the flow field.¹⁻³

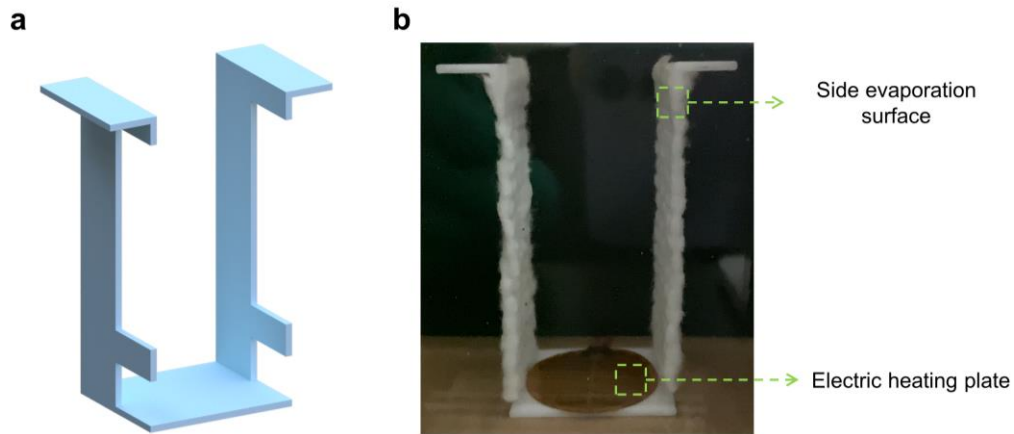


Figure S4. Structural simplification design for convective visualization. (a) Simplified structure design of the TIE. (b) The simplified design of the TIE physical image. In order to more intuitively display the convection situation inside the TIE, we simplified the original tower structure of the TIE to a U-shaped structure based on the use of flue gas visualization technology. At the same time, natural convection is generated by simulating the bottom photothermal layer with an electric heater. In additions, there are cold evaporation layers on both sides of the U-shaped structure that are the same in the TIE.

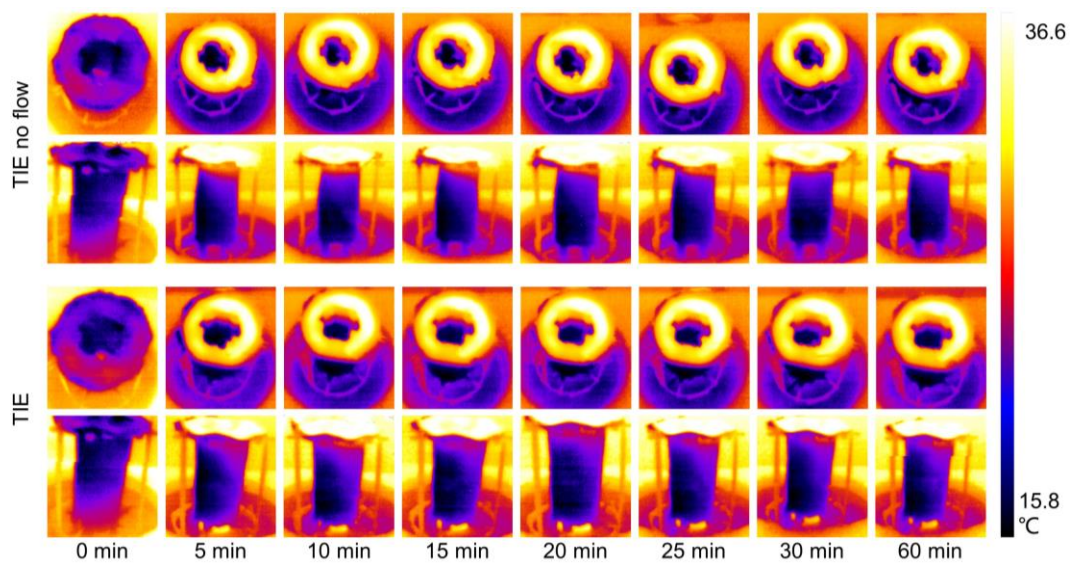


Figure S5. The infrared images of evaporation in the TIE or the TIE without flow.

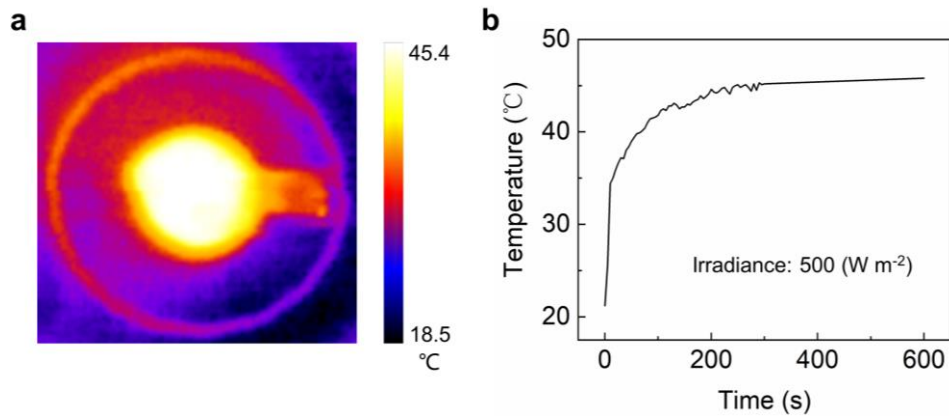


Figure S6. The temperature changes in the photothermal area under low sun intensity. (a) Infrared image of the photothermal area. (b) The variation of surface temperature over time in the photothermal area. There is a height difference of nearly 7 cm between the bottom photothermal area and the top interfacial evaporation area, resulting in one sun intensity of around 500 W m^{-2} in the bottom photothermal area. At this sun intensity in the photothermal area, the temperature can still be close to $45 \text{ }^{\circ}\text{C}$, which ensures the generation of natural convection.

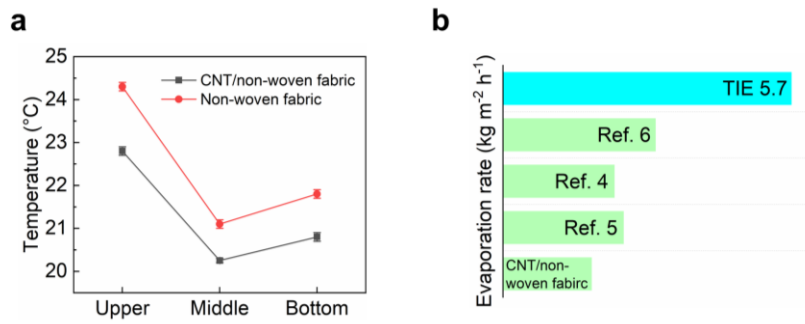


Figure S7. The advantages and performance comparison of CNT/non-woven fabrics. (a) Influence of CNT/ non-woven fabric and non-woven fabric on TIE side temperature, (b) Comparison of CNT/ non-woven, TIE and other work. Compared with non-woven fabric, CNT/non-woven fabric increases the side temperature of the TIE, which is beneficial to the side evaporation of the TIE.⁴⁻⁶

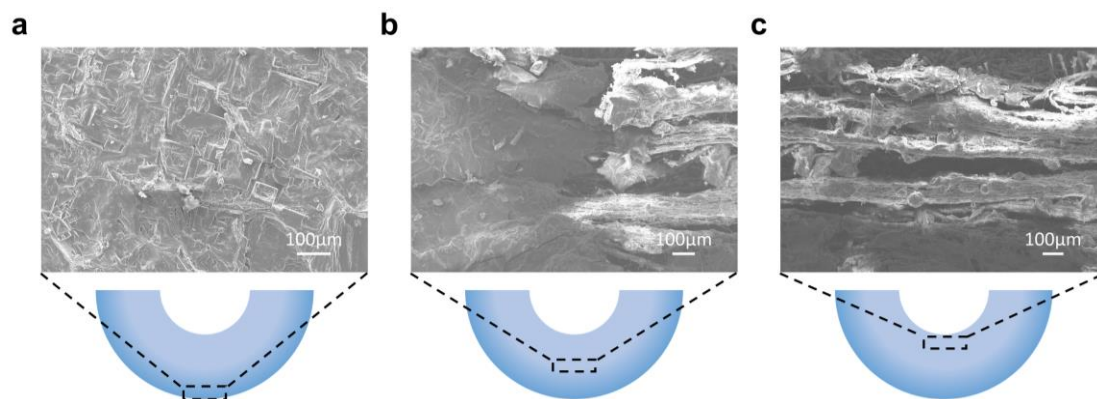


Figure S8. The salt distribution of the TIE after long-term evaporation under seawater conditions. (a)- (c) Accumulation of salt at different positions on the surface of the TIE after long-term evaporation. After 10 h of evaporation of the TIE under seawater conditions, salt accumulates mainly at the outer edge of the interfacial evaporation area. Only a small amount of salt accumulates in most of the interfacial evaporation regions.

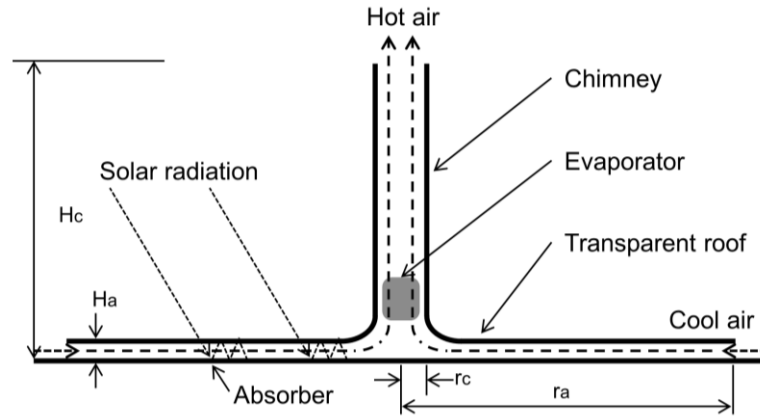


Figure S9. The overall design of the solar chimney. The chimney height H_c is 3 m, the chimney radius r_c is 10 cm, the bottom solar absorber radius r_a is 1.5 m, the transparent ceiling radius is 1.5 m, and the distance between the transparent ceiling and the bottom solar absorber height H_a is 6 cm.^{7,8}

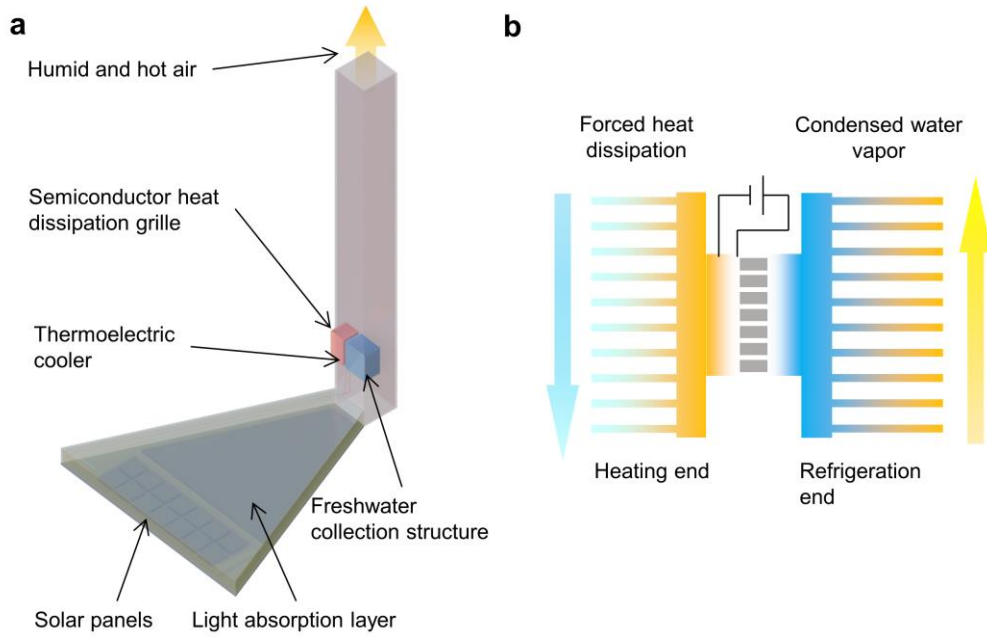


Figure S10. The initial idea of water vapor condensation and collection. (a) Design of water vapor condensation and collection structure based on solar chimney, (b) Schematic diagram of semiconductor refrigeration effect acting on water vapor condensation.

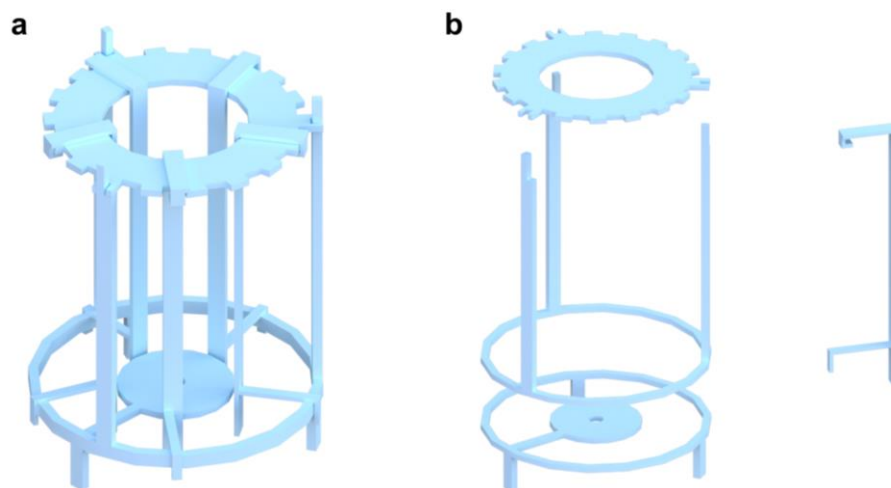


Figure S11. 3D printing framework of the TIE. (a) The overall structure of 3D printing framework of the TIE. (b) Exploded view of 3D printing framework of the TIE.

Table S1. List of materials for the solar chimney.

Materials	Size	Number	Coast (\$)
Aluminum Profile TDT-2020	0.5m	24	20.79
Aluminum Profile TDT-2020	0.3mm	12	6.24
Corner connector TDT-2020		24	5.02
DNS TDT-2020		6	2.18
Slotted strip TDT-2020		12	5.02
Expansion link	3m	1	2.02
Black insulation cotton	9m ²	1	7.59
Transparent PVC waterproof cloth	7m ²	1	10.78
Ventilation duct	3m	1	2.27
Evaporator		1	Homemade

The total amount is 69.91 US dollars.

Supplementary Note 1. Ideal gas law and Dalton's law.

Ideal gas law:

$$pV = nRT$$

p is the pressure (Pa), V is the gas volume (m^3), T is the temperature (K), n is the amount of gas substance (mol), and R is the molar gas constant ($\text{J mol}^{-1} \text{K}^{-1}$). Dalton's Law, which states that a gas in a gaseous medium has a partial pressure equal to that which would be exerted by that gas alone at a given temperature. It is obvious that the water vapour pressure is inversely proportional to the air's water vapour content at constant temperature and volume. Additionally, the vapour pressure refers to the pressure (partial pressure) of water vapour itself in humid air, which is the saturated vapour pressure when the air is saturated. As a result, the concentration of water molecules and the change in humidity are connected. Relative humidity refers to the ratio of the actual water vapour pressure in the air to the saturated water vapour pressure at the same temperature, so the change in humidity is related to the concentration of water molecules.

Supplementary Note 2. Numerical simulation.

Numerical simulations were conducted by COMSOL Multiphysics version 5.6. Multi-modules combining Laminar Flow, Fluid Heat Transfer and Moisture Transport in Air were applied to calculate the internal convection and humidity distribution during TIE evaporation.⁹ The intensity of natural convection can be reflected by the simulation results of the velocity magnitude. This node uses the following version of the heat equation to simulate heat transfer in fluids:

$$\rho C_p \frac{\partial T}{\partial t} + \rho C_p \mathbf{u} \cdot \nabla T + \nabla \cdot (-k \nabla T) = Q$$

Among them, ρ is the fluid density. C_p is the fluid heat capacity at constant pressure ($\text{J kg}^{-1} \text{K}^{-1}$). k is the thermal conductivity of the fluid ($\text{W m}^{-1} \text{K}^{-1}$). \mathbf{u} is the fluid velocity field (m s^{-1}). Q is the heat source (W m^{-3}).

The following node is used to simulate water transfer in humid air through vapour diffusion and convection. For low vapour concentration conditions, the density of moist air should not change with the change in moisture content, and a diluted substance formula is used. In this case, the change in moisture content is represented by the transfer of vapour concentration:

$$M_v \frac{\partial c_v}{\partial t} + M_v \mathbf{u} \cdot \nabla c_v + \nabla \cdot \mathbf{g}_w = G$$

$$\mathbf{g}_w = -M_v D \nabla c_v$$

$$c_v = \phi_w c_{sat}$$

Whereby, M_v is the Molar mass of water vapor (kg mol^{-1}). ϕ_w is relative humidity. c_{sat} is the saturation concentration of steam (mol m^{-3}). D is the diffusion coefficient of steam in the air ($\text{m}^2 \text{s}^{-1}$). \mathbf{u} is the air velocity field (m s^{-1}). G is the water source ($\text{kg m}^{-3} \text{s}^{-1}$).

References:

- 1 X. Wei, Y. Liu, G. Xie, W. Chen and Z. Jiang, *Sol. Energy*, 2023, **252**, 145-155.
- 2 M. Hamdi, M. Havet, O. Rouaud and D. Tarlet, *Exp. Fluids*, 2014, **55**, 1-12
- 3 N. I. Mikheev, A. E. Goltsman, I. I. Saushin and O. A. Dushina, *Exp. Fluids*, 2017, **58**, 1-10.
- 4 P. He, H. Bai, Z. Fan, L. Hao, N. Liu, B. Chen, R. Niu and J. Gong, *J. Mater. Chem. A*, 2022, **10**, 13378-13392.
- 5 N. Liu, L. Hao, B. Zhang, R. Niu, J. Gong and T. Tang, *Energy Environ. Mater.*, 2022, **5**, 617-626.
- 6 X. Song, W. Dong, Y. Zhang, H. M. Abdel-Ghafar, A. Toghan and H. Jiang, *Exploration*, 2022, **2**, 20220054
- 7 M. Ghalamchi, A. Kasaeian, M. Ghalamchi and A. H. Mirzahosseini, *Renew. Energ.*, 2016, **91**, 477-483.
- 8 A. B. Kasaeian, S. Molana, K. Rahmani and D. Wen, *Renew. Sust. Energ. Rev.*, 2017, **67**, 954-987.
- 9 R. Fillet, V. Nicolas, A. Celzard and V. Fierro, *Chem. Eng. J.*, 2023, **457**, 141168.